Recursive Subspace Identification for Online Thermal Management of Implantable Devices

Ayca Ermis
School of ECE
Georgia Tech
Atlanta, GA, USA
aycaermis@gatech.edu

Yen-Pang Lai
School of ECE
Georgia Tech
Atlanta, GA, USA
yenpang_lai@gatech.edu

Xinhai Pan
School of ECE
Georgia Tech
Atlanta, GA, USA
xpan78@gatech.edu

Ruizhi Chai
School of ECE
Georgia Tech
Atlanta, GA, USA
rchai3@gatech.edu

Ying Zhang
School of ECE
Georgia Tech
Atlanta, GA, USA
yzhang@gatech.edu

***Abstract*—This paper focuses on application of subspace identification methods to predict the thermal dynamics of bio-implants, e.g. UEA. Recursive subspace identification method implemented in this paper predicts the temperature readings of heat sensors in an online fashion within a finite time window and updates the system parameters iteratively to improve the performance of the algorithm. Algorithm validation is realized using COMSOL software simulations as well as using an in vitro experimental system. Both simulation and experimental results indicate that the proposed method can accurately predict the thermal dynamics of the system. The experimental results show online prediction of the thermal effect with a mean squared error of 1.569×10^{-2}°C for randomly generated Gaussian inputs and 3.46×10^{-3}°C for square wave inputs after adaptive filters converge.**

***Index Terms*—subspace identification, predictive modeling, implantable medical device, thermal effect**

I. Introduction

Implantable medical devices (IMDs) have become increasingly important in the modern society due to their increased functionality in monitoring, recording neural signals and providing required stimulation for medical purposes. Such improved capabilities of IMDs require higher power consumption and can potentially lead to overheating in the surrounding tissue of IMDs in certain applications, such as neural prostheses deep brain stimulators (DBS). Many neural prostheses need to constantly stimulate the body with electrode arrays and communicate with external devices continuously for monitoring and recording purposes. As a result, continuous operation of such implantable devices for long periods of time can cause a temperature increase that is significant. European standards for active IMDs require that the maximum temperature difference between the outer surface of the implant and the normal body should not exceed 2°C [1]. An example of the detrimental thermal effect of neural prostheses discussed in [2] and [3] is that a patient with implanted DBS suffered a serious brain damage due to overheating in brain tissue surrounding the DBS and subsequently died.

Online prediction of the thermal effect caused by an implantable medical device is essential for the real-time thermal management. In [4], finite element analysis (FEA) and finite difference time domain (FDTD) are proposed to solve the Pennes bioheat equation which models the thermal effect of IMDs. The aforementioned numerical methods solve for the heat dissipation and electromagnetic field for the whole computational domain for each time instance. Due to the space and time complexity of these numerical methods, they are not suitable for applications of real-time thermal management. In [5] and [6], Chai *et al.* proposes a recursive multi-step prediction error minimization method (RMSPEM) to update the model parameters online and achieve real-time thermal management of implantable devices. In their work, the thermal effect of a single heat source is investigated.

In this paper, an alternative method based on subspace identification is explored for modeling the thermal dynamics of the implantable device with multiple heat sources. Substantial progress has been made to identify an LTI state-space model of a dynamic system from system inputs and corresponding measurements, an example of which is presented in [7]. Online prediction algorithm used in this paper is based on the predictor-based subspace identification (PBSID) method, proposed in [8]. The algorithm presented in [8] uses the high-order vector auto-regressive with exogenous inputs (VARX) predictor from [7], since the performance of the VARX predictor compares favorably to other subspace identification algorithms [9]. In our application, we implement this subspace identification algorithm with a first order VARX predictor to model slowly time-varying parameters of a multiple-input system. Performance of the algorithm implemented in this paper is comparable to the performance of the RMSPEM algorithm proposed in [5] and [6], while having a relatively lower computational cost.

An implantable neural prosthetics based on UEA is used to evaluate the implemented online thermal prediction algorithm. UEA is chosen as the bio-implant since it has become a benchmark for neural recording and its thermal effect has been investigated in previous literature [10]. As described in [6], the UEA consists of radio, power, and motherboard module. Different from the previous work, there exists multiple heat sources whose power consumption can be controlled through the control input, and multiple temperature sensors

This work was supported in part by the National Science Foundation under Grant ECCS-1711447 and Grant CNS-1253390.

spatially distributed on the motherboard. We consider that each temperature sensor measures the temperature change of a subsystem and assume in this paper that the spatial correlation of the overall system can be implicitly solved by modeling the overall system as a combination of subsystems as shown in Figure 1. Thus, it would be possible to investigate the performance of PBSID algorithm on characterizing the thermal effect of the implantable devices with multiple heat sources.

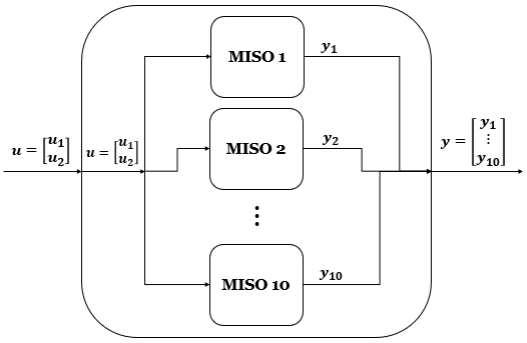

Fig. 1: Illustration of the overall system diagram.

II. Online Prediction Algorithm

For each subsystem S_i, the dynamics can be written as the following state-space model:

$$\begin{aligned} x_{k+1} &= Ax_k + Bu_k + w_k \\ y_k &= Cx_k + Du_k + v_k \end{aligned} \tag{1}$$

where $x_k, w_k \in \mathbb{R}^n$, $u_k \in \mathbb{R}^r$, $y_k, v_k \in \mathbb{R}^l$. w_k and v_k are process noise and measurement noise vectors respectively. We assume w_k and v_k are zero-mean Gaussian sequences. Using Kalman filter theory, we can correlate the noise vectors w_k and v_k via a Kalman gain K. Then, we can re-formulate (1) into the innovation form as follows

$$\begin{aligned} \hat{x}_{k+1} &= A\hat{x}_k + Bu_k + Ke_k \\ y_k &= C\hat{x}_k + Du_k + e_k \end{aligned} \tag{2}$$

where $\hat{x}_k \in \mathbb{R}^n$ denotes the predicted state vector with expected value of state error equals to zero. $e_k \in \mathbb{R}^l$ denotes the zero-mean innovation sequence, and $K \in \mathbb{R}^{n \times l}$ is the Kalman gain. We use vector auto-regressive with exogenous inputs (VARX) model for the thermal dynamics of the multiple-input, single output (MISO) subsystem. One-step-ahead VARX predictor can be written as

$$\hat{y}_{k|k-1} = \sum_{i=0}^{p} \alpha_i u_{k-i} + \sum_{i=1}^{p} \beta_i y_{k-i} \tag{3}$$

where $\hat{y}_{k|k-1}$ is the output of the subsystem at time instant k predicted by the algorithm using a finite window of past inputs and outputs. p denotes the length of the finite window of past data. $\bar{\Xi}_k \in \mathbb{R}^{l \times p(r+l)+r}$ consists of VARX paramaters which need to be estimated.

$$\bar{\Xi} := \begin{bmatrix} \alpha_p & \alpha_{p-1} & \dots & \alpha_0 & \beta_p & \dots & \beta_1 \end{bmatrix} \tag{4}$$

Using VARX model, we can estimate Markov parameters of the system as shown in [11], [8].

A. Regularized Batch Pre-processing

Prior to online prediction, initial values for Markov parameters of the system are determined by using a batch of data. This procedure is called batch pre-processing. First step in batch pre-processing is to construct stacked matrices U, Y, and Hankel matrices for $\bar{Y}_p$ and $\bar{U}_p$ as shown in [8]. Using these stacked matrices, parameters of the linear VARX predictor in (3) can be estimated using least squares regression as follows:

$$\begin{aligned} \bar{\Xi} &= Y\Psi^{\dagger} \\ \Psi &= \begin{bmatrix} \bar{U}_p^T & U^T & \bar{Y}_p^T \end{bmatrix}^T \end{aligned} \tag{5}$$

where $(.)^{\dagger}$ denotes pseudo-inverse of the matrix.

Tikhonov regularization introduced in [12] is applied to the batch pre-processing by modifying (5) with $\bar{\Xi} = Y\Psi^T(\Psi\Psi^T + \mu I)^{-1}$ where μ is the regularization term selected to minimize the estimation error.

Once the VARX predictor parameters $\bar{\Xi}$ is computed, product of the extended observability matrix and state sequence, $\widehat{\Gamma X}$, can be estimated from input-output data using the extended observability and controllability matrices, $\widetilde{\Gamma L}$ and $\widetilde{\Gamma K}$, that are constructed from $\bar{\Xi}$. Since the size of our future window is $f = 1$, $\widetilde{\Gamma L}$ and $\widetilde{\Gamma K}$ for our subsystems would be

$$\begin{aligned} \widetilde{\Gamma L} &= \begin{bmatrix} \alpha_p & \alpha_{p-1} & \dots & \alpha_1 \end{bmatrix} \\ \widetilde{\Gamma K} &= \begin{bmatrix} \beta_p & \beta_{p-1} & \dots & \beta_1 \end{bmatrix} \end{aligned} \tag{6}$$

Using the matrices in (6), we compute the state sequence as follows

$$\widehat{\Gamma X} = W(\widetilde{\Gamma L}\bar{U}_p + \widetilde{\Gamma K}\bar{Y}_p) \tag{7}$$

where W matrix is the weighting matrix. For simplicity, we assume $W = I$. We derive the predicted full state sequence $\hat{X}$ from $\widehat{\Gamma X}$ sequence by solving the low-rank approximation with SVD

$$\begin{aligned} \widehat{\Gamma X} &= \begin{bmatrix} U_n & U_{\perp} \end{bmatrix} \begin{bmatrix} S_n & 0 \\ 0 & S \end{bmatrix} \begin{bmatrix} V_n \\ V_{\perp} \end{bmatrix} \\ \hat{X} &= S_n^{\frac{1}{2}} V_n \end{aligned} \tag{8}$$

System matrices A, B, C, D, and the Kalman gain K can then be computed by solving the second linear problem in (1) with least squares method

$$\begin{bmatrix} C & D \end{bmatrix} = Y \begin{bmatrix} \hat{X} \\ U \end{bmatrix}^{\dagger} \tag{9}$$

With matrices C and D, innovation sequence $\hat{E}$, i.e. estimation error of the output y, can be calculated by subtracting the estimated output from the measured output ($\hat{E} = Y - (C\hat{X} +$

DU)). With the estimation error, the first linear problem in (1) is solved as follows

$$\begin{bmatrix} A & B & K \end{bmatrix} = \hat{X}' \cdot \begin{bmatrix} \hat{X} \\ U \\ \hat{E} \end{bmatrix}^{\dagger} \tag{10}$$

where $\hat{X}'$ is the stacked matrix $\hat{X}$ shifted one time instant to right to capture the next state.

B. Recursive PBSID with Projection Approximation Subspace Tracking (PAST) Method

Recursive predictor-based subspace identification (RPBSID) method updates the model parameters iteratively. For this method, the system matrices and Kalman gain obtained from batch pre-processing is used for initialization of these model parameters.

Adaptive filters, more specifically recursive least squares (RLS) filters, are implemented to track time-varying dynamics of the system, and a forgetting factor is added to ensure that the weight of the past data is reduced for the current estimation.

For recursive prediction, VARX predictor in (3) is rewritten in the linear regression form

$$y_k = \tilde{\Xi}_k \psi_k + e_k \tag{11}$$

where $\psi = \begin{bmatrix} {u_p}^T & {u_k}^T & {y_p}^T \end{bmatrix}^T$, u_p and y_p are the vectors of past p data points at time instant k. Different from batch pre-processing, $\tilde{\Xi}$ is defined as an adaptive filter of the form

$$\tilde{\Xi}_k = \tilde{\Xi}_{k-1} + (y_k - \tilde{\Xi}_{k-1}\psi_k){\psi_k}^T P_k \tag{12}$$

Error covariance matrix P_k is initialized at $P_i = (\frac{1}{\rho_1})I$ with $\rho_1 > 0$ and P_k is updated iteratively with

$$P_k = \frac{1}{\lambda_1}(P_{k-1} - P_{k-1}\psi_k(\lambda_1 I + {\psi_k}^T P_{k-1}\psi_k)^{-1}{\psi_k}^T P_{k-1})$$

where $1 \geqslant \lambda_1 \gg 0$ is the forgetting factor. Common values for the forgetting factor λ are between $0.95 < \lambda < 0.995$; thus, $\lambda = 0.99$ is selected for all RLS filters in the algorithm.

State vector $\hat{x}_k$ can then be estimated from the past input-output data, i.e. u_p and y_p, using the extended observability and controllability matrices similar to (7). More specifically, at time instant k,

$$\hat{x}_k = S(\widetilde{\Gamma L} u_p + \widetilde{\Gamma K} y_p) \tag{13}$$

where selection matrix S is determined via projection approximation subspace tracking (PAST) method in [13] and has an adaptive filter update. From the estimated state vector $\hat{x}_k$, system matrices A_k, B_k, C_k, D_k, and the Kalman gain K_k are computed by updating the following two RLS filters

$$\begin{aligned} \begin{bmatrix} C_k & D_k \end{bmatrix} &= \begin{bmatrix} C_{k-1} & D_{k-1} \end{bmatrix} \\ &+ (y_{k-1} - \begin{bmatrix} C_{k-1} & D_{k-1} \end{bmatrix} \phi_{k-1}) \phi_{k-1}^T M_k \end{aligned} \tag{14}$$

$$\begin{aligned} \begin{bmatrix} A_k & B_k & K_k \end{bmatrix} &= \begin{bmatrix} A_{k-1} & B_{k-1} & K_{k-1} \end{bmatrix} \\ &+ (\hat{x}_{k-1} - \begin{bmatrix} A_{k-1} & B_{k-1} & K_{k-1} \end{bmatrix} \theta_{k-1}) \theta_{k-1}^T N_k \end{aligned} \tag{15}$$

where $\phi_k = \begin{bmatrix} \hat{x}_k^T & {u_k}^T \end{bmatrix}^T$ and $\theta_k = \begin{bmatrix} \hat{x}_k^T & {u_k}^T {e_k}^T \end{bmatrix}^T$ with estimation error $e_k = y_k - \begin{bmatrix} C_k & D_k \end{bmatrix} \phi_k$. N_k and M_k are error covariance matrices associated with each RLS filter with an update similar to P_k.

III. Algorithm Validation

A. Simulation Studies

Multiphysics modeling software COMSOL is used to simulate the thermal dynamics of the UEA. Modelling of the UEA, presented in [10], with multiple heat sources is achieved in the COMSOL software as shown in Figure 2. Simulation board includes two heat sources (H1 and H2) and six probes, (S1-S6), to measure the temperature change. The probes are placed at $(x, y, z) = \{(-0.025, 0, 0.673), (-0.025, -0.025, 0.673), (-0.025, 0.025, 0.673), (0.025, 0, 0.673), (0.025, -0.025, 0.673), (0.025, 0.025, 0.673)\}$ surrounding two heat sources. Temperature readings produced by the COMSOL software is used as a reference to demonstrate the performance of the online prediction algorithm.

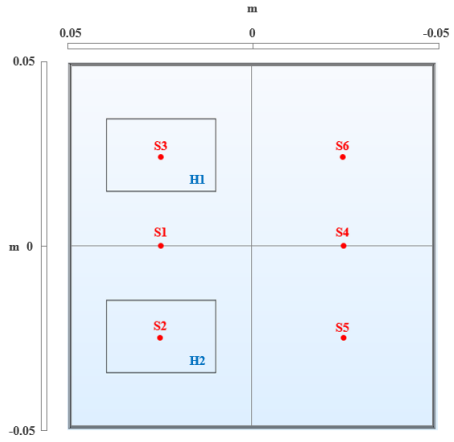

(a)

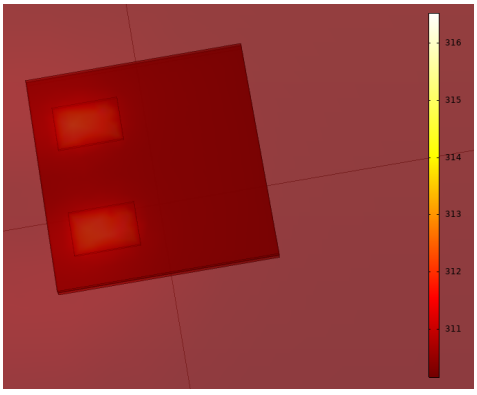

(b)

Fig. 2: (a) PCB layout in COMSOL software with sensors locations in *red*, (b) illustration of the developed COMSOL model and its surface temperature distribution in Kelvin.

Two sets of studies were conducted using the aforementioned COMSOL model: (1) 1800 data samples generated using two Gaussian distributions within the range of $[0, 0.837]$ Watt (W) are used for the power inputs in the first simulation;

and (2) for the second simulation, square wave signals of length 1800 are used to emulate the controller effect on the power input and evaluate the performance of the prediction algorithm when controller is implemented. The range of the Gaussian distributions in study (1) denotes the range of operating power inputs. In study (2), square wave signals for both inputs have the same 50% duty cycle and a period of 20 seconds. For each simulation study, two separate runs are conducted to examine the thermal effect of applying same vs. different power inputs to the two heat sources. In study (2), square wave inputs of amplitude 0.25 W are generated for the case with same inputs. For the case with different amplitudes in study (2), one of the square wave inputs has an amplitude of 0.25 W and the other input has an amplitude of 0.125 W. In Figure 3, comparison results when Gaussian inputs of different amplitudes are applied, are shown. More specifically, in Figure 3(a), the power inputs are displayed, and in Figure 3(b), comparison between results of the online prediction algorithm (in red) and temperature readings of the COMSOL model corresponding to each subsystem (in blue) is shown. Figure 4 shows the corresponding results for the square wave inputs with different amplitudes.

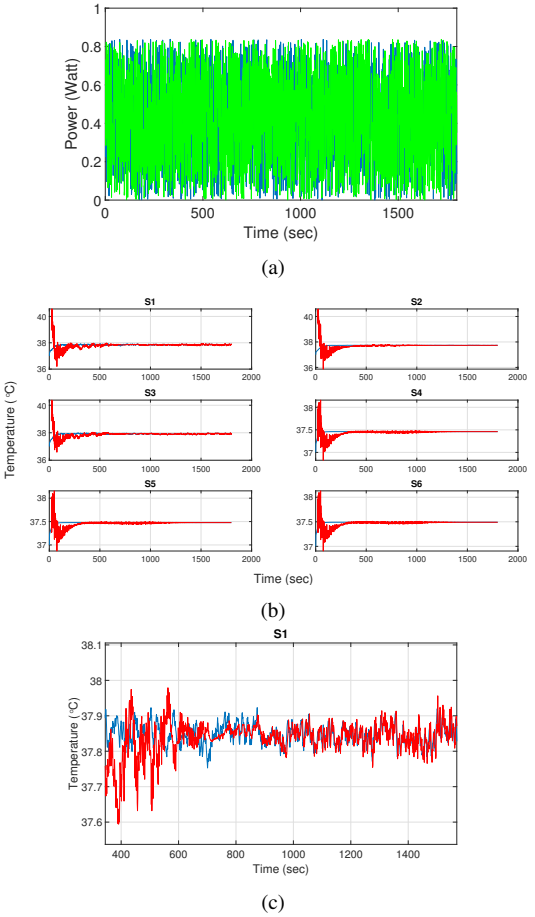

Fig. 3: (a) Different randomly generated Gaussian inputs, (b) Simulation results, and (c) Simulation results (zoomed-in)

The comparison between the results of the online prediction algorithm and the temperature readings obtained in

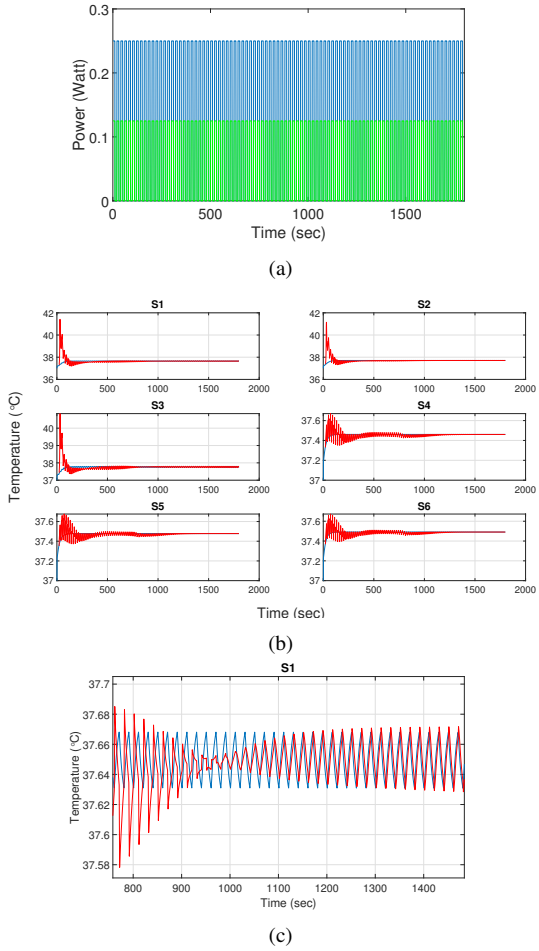

Fig. 4: (a) Square-wave inputs with different amplitudes of 0.125 W *(green plot)* and 0.25 W *(blue plot)* respectively, (b) Simulation results, and (c) Simulation results (zoomed-in)

COMSOL shows that the thermal dynamics of bio-implant with multiple heat sources, i.e. multiple power inputs, can be predicted by predictor-based subspace identification (PBSID) methods with relatively high accuracy. Mean square error for each of these sensor subsystems, indicated as S1, S2 etc., is summarized in Table I. Similar results are also obtained for the simulation studies when the same power input is applied to both heat sources, and the corresponding MSE is also listed in Table I. From the MSE in Table I, it can be concluded that the online prediction algorithm with 1st order VARX model predicts the thermal effect with an average mean squared error of 4.635×10^{-2}°C for randomly generated Gaussian inputs and 4.368×10^{-2} °C for square-wave inputs. After convergence of the adaptive filters are achieved, i.e after approx. 200 seconds for Gaussian inputs and 400 seconds for square-wave inputs, average mean squared error drops to 1.907×10^{-3}°C for Gaussian inputs and to 0.813×10^{-3} °C for square-wave inputs.

B. Experiments

Based on the previous hardware testing system used in [6], a new temperature monitoring and management test vehicle

TABLE I: Results of the simulation studies

		Gaussian Input		Square-Wave Input	
	S#	Same Inputs	Different Inputs	Same Inputs	Different Inputs
MSE ($\mathbf{x10^{-2}}$)	S1	10.66	8.21	9.81	10.85
	S2	9.52	9.43	7.41	8.48
	S3	7.74	6.36	7.37	7.66
	S4	0.54	0.79	0.18	0.13
	S5	0.50	0.73	0.16	0.12
	S6	0.46	0.68	0.14	0.10

(TMTV) is developed, which has seven temperature sensors (LMT70) and two heat sources emulating the implanted electronics. This version of the TMTV is smaller compared to the previous T-shaped version used in [5] and more compact in size and shape.

A Matlab GUI, integrated with the online prediction algorithm, is created to display and save the temperature measurements and prediction results simultaneously. Continuous temperature data and prediction results for multiple subsystems can also be displayed simultaneously in the GUI. This Matlab front-end is connected with an nRF52 board, which acts as the intermediate layer between the TMTV and PC interface. The nRF52 board sends control signals to both heat sources on the TMTV, and captures the temperature readings from the TMTV and then transmits them to PC. The current hardware testing system is shown in Figure 5.

Fig. 5: Developed TMTV system

Two sets of experiments were conducted with this hardware testing system to evaluate the performance of the prediction algorithm. For all experiments, a training data is used for the batch pre-processing such that the recursive PBSID updating can be initiated after 10 seconds of the input and output data are obtained. Heat sources on TMTV admit PWM inputs within the range of $[0, 10000]$ where 10000 denotes a PWM signal with 0% duty cycle and 0 denotes a PWM signal with 100% duty cycle. For the first set of experiments, two separate runs are conducted to examine the thermal effect of applying same vs. different Gaussian PWM inputs to the two heat sources. In the first run, 1100 data samples generated using a Gaussian distribution within the range of $[1620, 10000]$ are used for both PWM inputs. For the case of Gaussian PWM inputs with different amplitudes, 2000 data samples are generated using two Gaussian distributions within the range of $[5000, 10000]$ and $[7500, 10000]$ individually. For the second set of experiments, square wave inputs of length 2000 are used to evaluate the performance of the prediction algorithm when controller is implemented in real applications. Square wave inputs have the same 50% duty cycle and a period of 20 seconds. The ranges of the square wave PWM inputs with different amplitudes are $[7500, 10000]$ and $[8750, 10000]$ respectively. For the PBSID prediction algorithm, normalized values of the PWM inputs are used.

Figure 6 shows the experiment results when randomly generated Gaussian inputs with different amplitudes are applied. More specifically, in Figure 6(a), PWM inputs and comparison between results of the online prediction algorithm (in red) and temperature readings from the corresponding sensor (in blue) are displayed, and in Figure 6(b) a zoomed-in version of results is shown. Results for the second set of experiments are shown for which square-wave inputs of different amplitudes are applied in Figure 7; in (a) PWM inputs and experiment results can be seen, and in (b) a zoomed-in version of results is displayed to emphasize the performance of the prediction algorithm.

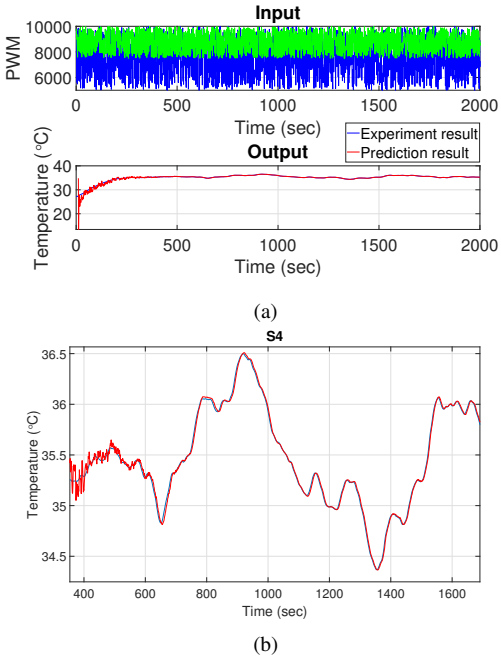

(a)

(b)

Fig. 6: (a) different Gaussian inputs and experiment result, (b) Experiment result (zoomed-in)

Mean squared error for all MISO subsystems, indicated as S1, S2 etc., corresponding to each simulation study is summarized in Table II. From the MSE in Table II, it can be concluded that the online prediction algorithm with 1st order VARX model predicts the thermal effect with an average mean squared error of $2.779 \times 10^{-1} {}^{\circ}C$ for randomly generated Gaussian PWM inputs with different amplitudes and $3.277 \times 10^{-1} {}^{\circ}C$ for square-wave PWM inputs with different amplitudes. After convergence of the adaptive filters are achieved, i.e after approx. 100 seconds, average mean squared error drops to $2.179 \times 10^{-2} {}^{\circ}C$ for Gaussian inputs,

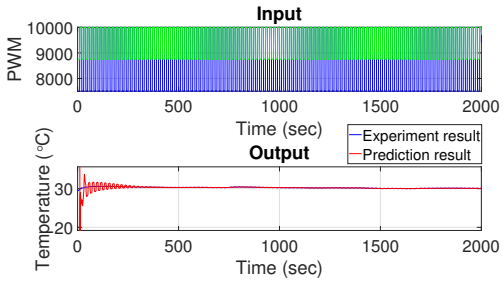

(a)

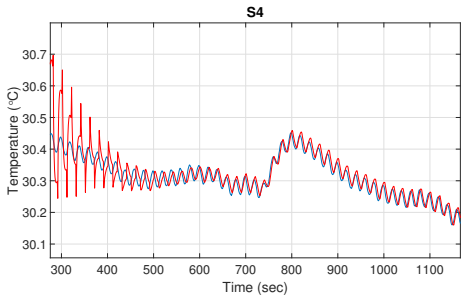

(b)

Fig. 7: (a) Square-wave inputs with different amplitudes and experiment result, (b) Experiment result (zoomed-in)

TABLE II: Results of the experiments

	S#	**Gaussian Input** Different PWM Inputs	**Square-Wave Input** Different PWM Inputs
MSE	S1	0.320	0.406
	S2	0.255	0.288
	S3	0.292	0.356
	S4	0.260	0.283
	S5	0.275	0.317
	S6	0.282	0.343
	S7	0.272	0.301

and to $2.993 \times 10^{-2}{}^{\circ}C$ for square-wave inputs. Although experiment results have relatively higher mean squared error values compared with the COMSOL simulation studies, it is acceptable for our application since the squared error results are significantly less than the critical temperature increase.

IV. Conclusion

With the emergence of complex implantable devices in medical field, thermal management of such devices has gained importance to ensure safe operation. In this paper, we implemented the recursive predictor-based subspace identification method to predict the temperature increase due to continuous operation of the implantable medical device in an online fashion. Different from the previous work, which focuses mainly on the thermal effect of a single heat source, our paper examines the prediction of temperature increases caused by multiple heat sources. The presented algorithm predicts the temperature increase and iteratively updates Markov parameters of the system according to the recent input and output data. To validate the prediction algorithm, a COMSOL model of the implantable device is created and an experiment system emulating the neural prosthesis is built. Both COMSOL simulations and *in vitro* experiments demonstrate that the PBSID prediction algorithm with the 1st order VARX model predicts the thermal effect of the implantable device with high accuracy. Performance of the prediction algorithm increases significantly after adaptive filters converge. As a result, recursive PBSID algorithm with regularized batch pre-processing can successfully characterize the thermal effect of the implantable device with multiple heat sources.

References

[1] "Active Implantable Devices - Part 1: General requirements for safety, marking and information to be provided by the manufacturer," BS EN 45502-1:2015, European Standard, 2015.

[2] P. S. Ruggera, D. M. Witters, G. von Maltzahn, and H. I. Bassen, "In vitro assessment of tissue heating near metallic medical implants by exposure to pulsed radio frequency diathermy, Physics in Medicine and Biology, vol.48, pp.2919-2928, 2003.

[3] J. G. Nutt, V. C. Anderson, J. H. Peacock, J. P. Hammerstad, and K. J. Burchiel, DBS and diathermy interaction induces severe CNS damage," Neurology, vol.56, no.10, pp.1384-1386, 2001.

[4] S. C. DeMarco, G. Lazzi, W. Liu, J. D. Weiland, and M. S. Humayun, "Computed SAR and thermal elevation in a 0.25-mm 2-D model of the human eye and head in response to an implanted retinal stimulator-Part I: Models and methods," IEEE Transactions on Antennas and Propagation, vol.51, no.9, pp.2274-2285, 2003.

[5] R. Chai, Y. Lai, W. Sun, M. Ghovanloo, and Y. Zhang, "Online Predictive Modeling for the Thermal Effect of Implantable Devices," Proc. of 2018 IEEE Biomedical Circuits and Systems Conference (BioCAS), 2018.

[6] R. Chai, Y. Zhang, "Adaptive Thermal Management of Implantable Device," IEEE Sensors Journal, vol. 19, issue 3, pp.1176 - 1185 2018.

[7] A. Chiuso, "The role of vector auto regressive modeling in predictor based subspace identification", Automatica, vol. 43, issue 6, pp.1034-1048, 2007.

[8] I. Houtzager, J. van Wingerden, and M. Verhaegen, "Recursive Predictor-Based Subspace Identification With Application to the Real-Time Closed-Loop Tracking of Flutter," IEEE Transactions on Control Systems Technology, vol. 20, issue 4, pp.934 - 949, 2012.

[9] L. Ljung, T. McKelvey, "Subspace identification from closed loop data," Signal Process., vol. 52, pp. 209215, 1996.

[10] S. Kim, P. Tathireddy, R. A. Normann, and F. Solzbacher, "Thermal impact of an active 3-D microelectrode array implanted in the brain," IEEE Transactions on Neural Systems and Rehabilitation Engineering, vol.15, no.4, pp.493-501, 2007.

[11] A. Chiuso and G. Picci, "Consistency analysis of some closed-loop subspace identification methods," Automatica, vol. 41, no. 3, pp. 377391, 2005.

[12] A. N. Tikhonov, and V. Y. Arsenin, Solutions of Ill-Posed Problems. New York: Wiley, 1977.

[13] B. Yang, "Projection approximation subspace tracking," IEEE Transactions on Signal Processing, vol. 43, no. 1, pp. 95107, 1995.